CONF-811162--9

LA-UR -81-675

MASTER

TITLE: AQUARIUM TESTS ON ALUMINIZED ANFO

AUTHOR(S): S. Goldstein and J. N. Johnson

SUBMITTED TO: 7th Symposium (Internation l) on Detonation

University of California

LOS ALAMOS SCIENTIFIC LABORATORY
Post Office Box 1663 Los Alamos, New Mexico 87545
An Affirmative Action/Equal Opportunity Employer

Form No. 836 R3
St. No. 2629
12/78

UNITED STATES
DEPARTMENT OF ENERGY
CONTRACT W-7405-ENG. 36

AQUARIUM TESTS ON ALUMINIZED ANFO

S. Goldstein and J. N. Johnson
Los Alamos National Laboratory
Los Alamos, New Mexico

Aquarium test data are presented on commercially available ANFO and 7.5 wt% aluminized ANFO in 10-cm-i.d. clay pipe. The data obtained on the aluminized product show only slight measurable improvement in performance over the nonaluminized product, possibly because of inadequate control on initial sample density. Therefore, additional experiments were conducted on aluminized ANFO mixtures of our own composition to control initial sample density, aluminum concentration, and aluminum particle size. Direct measurement of shock pressures in the water were made with lithium niobate pressure transducers ∿28 cm from the charge. These tests show that the addition of aluminum (average particle size <100 μm) increases the peak pressure by more than 50% for the addition of 11 wt% aluminum to a standard (94/6) ANFO mixture. Tests conducted on 19 wt% aluminum showed a slightly smaller increase in peak pressure, indicating some optimal aluminum concentration for maximum shattering efficiency in blasting applications.

INTRODUCTION

A subject of current national interest is energy and mineral resource recovery, and an important part of this subject is controlled rock blasting with commercial explosives. As our predictive capabilities (1-4) in dynamic rock fracture improve, more detailed information on explosive behavior is required. Many explosive systems have been studied extensively and their behavior is well understood, following theoretical predictions based on steady-state detonation theory and equilibrium thermodynamics of the detonation products. Such explosive systems are said to behave ideally. Commercially available explosives, however, are usually nonideal. Their performance properties depend strongly on charge diameter and confinement. Energy release and the effects of late-time chemical reaction are not predictable by currently available techniques. Therefore, a considerable amount of testing under conditions close to those found in field applications is required to adequately characterize a particular blasting agent.

The aquarium test (5) has been used for several years to determine the properties of commercial blasting agents such as ANFO (ammonium nitrate/fuel oil). The experimental technique consists of placing the explosive in a cylindrical tube (if necessary) surrounded by water, detonating the explosive from one end, and taking several photographic exposures (separated by ∿50 μs) of the shock wave in the water and the expansion of the tube/water interface as shown in Fig. 1. From these photographs we obtain information on the detonation velocity, C-J state, and the progress of the chemical reaction in and behind the detonation front (5).

Ammonium nitrate is a common constituent of many commercial blasting agents, and many tests have been performed on ANFO and related materials. Of particular interest is the comparison of commercially available ANFO and aluminized ANFO. The addition of aluminum is thought to improve both the shattering and heaving effects of the explosive. While it is known from underwater testing to improve the energy release at

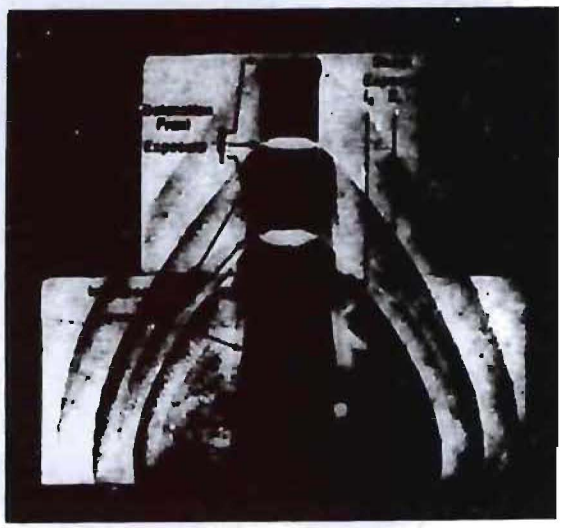

Fig. 1 - Aquarium test. Three photographic exposures taken with image intensifier camera. Visible are the detonation front, shock wave in water, and pipe (interface) expansion.

very late times after detonation, its earlier role has not been quantified.

In this paper we present a summary of aquarium test data on ANFO and aluminized ANFO contained in 10-cm-i.d. clay pipe (1.5 cm wall thickness). Since comparison of the commercially available aluminized product with nonaluminized ANFO proved difficult (density control, lack of information on the AN/FO mixture, and varying aluminum particle size), several aluminized ANFO products of our own composition were tested.

In addition to the established optical techniques (5) for determining explosive performance, lithium niobate stress transducers (6,7) were placed approximately 28 cm from the pipe wall to measure the dynamic pressure delivered to the surrounding medium (in this case water). The photographic record of the shock wave in water is also used to determine the peak pressure at the pipe/water interface.

AQUARIUM TESTS

Several types of ANFO and aluminized ANFO were tested in this study. The first was Gulf Oil Chemical Company Nitro-Carbo-Nitrate (N-C-N) 100, nominally 94% ammonium nitrate and 6% fuel oil by weight. The commercial aluminized ANFO product tested in this program was Gulf N-C-N 750, 7.5% aluminum by weight. The AN/FO composition for this explosive was unavailable. The remaining explosives tested here were 11 wt% and 19 wt% aluminized ANFO of our own composition, produced by mixing Gulf N-C-N 100 with aluminum particles (diam. 44-104 μm) supplied by Alloy Metals, Troy, MI. Mixture was accomplished by careful blending of the aluminum particles with ANFO prills that minimized crushing and produced a homogeneous composition. To ensure a realistic comparison, the nonaluminized product was also subjected to the mixing process.

In all tests reported here the explosives were poured into 120-cm-long, 10-cm-i.d. clay pipes (wall thickness ∿ 1.5 cm). The cylindrical charges were detonated from one end with a 10-cm-diam. plane wave lens in contact with a 10-cm-diam., 2.5-cm-thick disc of Composition B. The detonation front, water shock, and clay pipe/water interface were photographed with a multiple exposure, image-intensifier camera (I^2C) manufactured at Los Alamos National Laboratory (8). The exposure times in all experiments were ∿175 ns.

Measurement of shock pressure in the water was made with 6.35-mm-diam., 0.635-mm-thick lithium niobate discs (manufactured by Specialty Engineering, Santa Clara, CA) operated in the charge mode (6). This gauge has a resolving time on the order of 200 ns (double transit time through the gauge thickness) and a charge output of 6.31×10^{-8} c/cm^2 kbar. Thus, when the voltage V from a 6.35-mm-diam. gauge is recorded across a 0.01-μf capacitor the pressure is given by p(kbar) = 0.500 V (volts). The gauges were located 28 cm from the outer wall of the clay pipe, mounted on 60-mil-thick, thin aluminum supports and oriented parallel to the shock front. The aquarium setup with stress gauges in place is shown in Fig. 2. The aquarium measures 106 cm by 91 cm by 91 cm high. Gauges are approximately 60 cm above the floor of the aquarium, so that they will not see disturbances caused by the detonator-booster system at the top of the pipe, or by reflected waves from the aquarium floor.

To calibrate the gauge readings and to test them in the aquarium environment, we performed a small-scale proof test using nitromethane in a 1-in.-i.d. Teflon tube, for which accurate calculations of pressure as a function of distance were performed with the two-dimensional Lagrangian code 2DL (9). Several gauges were used in the charge mode to confirm reproducibility and stability under the experimental conditions, and

Fig. 2 - Setup of aquarium test prior to top detonation. Three lithium niobate gauges on aluminum supports are shown mounted on the bottom of the tank.

one in the current mode (6) to check the reading of the peak pressure. The calculated angle of the shock front from the vertical was used to orient the gauges for plane incidence. Results are shown in Fig. 3.

A comparison of the gauge readings indicate that the charge-mode gauges record the peak pressure after a several-hundred-nanosecond rise time as expected. Both modes then record a maximum pressure of about 3 kbar at 8 cm from the pipe wall. This agrees reasonably well with the calculated pressure at this position.

EXPERIMENTAL RESULTS

A list of ten aquarium tests on ANFO, all contained in 10-cm-i.d. clay pipe is given in Table 1. Lithium niobate gauge records were obtained in three cases: 0, 11%, and 19% aluminum by weight. Peak pressures recorded at 28 cm from the pipe wall are listed as P_{gauge}. The average pipe wall velocity $\bar{V}$ and the detonation speed D are also given. The calculated peak pressure, P_{wall}, at the outer wall of the clay

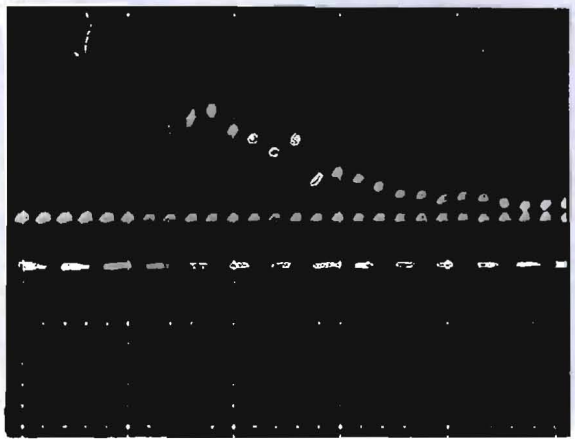

Fig. 3 - Lithium niobate gauge record from small-scale nitromethane aquarium test. The vertical scale is 5 V (2.5 kbar) per division and the horizontal scale is 20 μs per division.

pipe is determined by measurement of the shock angle with respect to the pipe wall and knowledge of the equation of state of water, as described in the Appendix.

The aquarium tests on zero wt% aluminum show the expected general tendency of improved explosive performance (as measured by $\bar{V}$ and P_{wall}) with increased packing density. It can be seen that the 7.5 wt% aluminized ANFO experiment, C-4724, has a slightly higher average wall velocity, but its calculated pressure P_{wall} is considerably less than comparable nonaluminized products, particularly C-4652. It was for this reason that further tests were performed on aluminized ANFO explosives of our own composition, and the major reason that direct measurement was made of the shock pressure imparted to the surrounding medium.

Because of the influence of initial density of nonaluminized ANFO on explosive performance, it is important to choose some reasonable standard for density variation in the aluminized products. One particular standard is to choose initial density (ANFO plus aluminum) in such a way that the density of the ANFO remains constant and the aluminum particles fill the interstitial positions between the fuel-soaked ammonium nitrate prills. If W is the mass fraction of aluminum and ρ_s is the pour density of nonaluminized ANFO, the initial density of the aluminized product is chosen to be

$$\rho = \rho_0/(1 - W) \qquad (1)$$

TABLE 1
Summary of Aquarium Tests on ANFO and Aluminized ANFO in 10-cm-diameter Clay Pipe (1.5-cm wall thickness)

Shot No.	Aluminum Content, W wt%	ρ g/cm^3	D (mm/μs)	$\bar{V}$ (mm/μs)	P_{wall} (kbar)	P_{gauge} (kbar)
C-5084	0	0.76	2.88	0.30	7.1	2.3
C-4678	0	0.79	3.27	0.34	8.9	---
C-5058	0	0.80	3.33	0.34	9.9	---
C-4652	0	0.90	3.47	0.37	12.7	---
C-4768	0	0.93	3.56	0.39	11.2	---
C-4724	7.5*	0.87	3.63	0.42	9.3	---
C-5088	11†	0.80	3.2	0.36	8.5	3.8
C-5061	11†	0.85	3.75	0.35	13.5	---
C-5097	19†	0.90	3.51	0.41	11.3	3.6
C-5066	19†	0.93	3.50	0.41	13.4	---

*Gulf N-C-N 750.

†Gulf N-C-N 100 mixed with <100 μm aluminum particles at Los Alamos National Laboratory.

in order to keep the ANFO prill density constant in comparison of aluminized and nonaluminized cases. There may be other reasonable standards by which to compare aluminized and nonaluminized blasting agents, but they are not investigated here.

In experiment C-5084 (0% aluminum) the initial density is $\rho_0 = 0.76$ g/cm^3. For comparison with 7.5%, 11%, and 19% aluminized products the densities should be, according to Eq. (1), 0.82 g/cm^3, 0.85 g/cm^3, and 0.94 g/cm^3, respectively. The 7.5% test, C-4724, has an initial density that is too large; part of the improved performance, if any, can be attributed to this higher density (0.87 g/cm^3 instead of 0.82 g/cm^3). However, it is reasonable to compare C-5061 (11% aluminum) and C-5066 (19% aluminum) with each other and with C-5084. Although gauge records are not available for C-5061 and C-5066, the calculated peak wall pressures show an increase from 7.1 kbar to >13 kbar for the addition of aluminum, a very significant effect.

Lithium niobate stress gauge records were obtained in three tests: C-5084, C-5088, and C-5097. Although the initial densities do not follow Eq. (1), and comparison of different aluminum percentages becomes more difficult, it is clear that the addition of aluminum significantly improves explosion performance. The peak shock pressure at 28 cm from the pipe wall is increased by a factor of 1.65 for 11% aluminum, and by slightly less than this for 19% aluminum.

The complete oscilloscope records of the lithium niobate gauge outputs in shots C-5084, C-5088, and C-5097 are shown in Fig. 4. The differences in arrival times are real. The arrival of the shock wave at the gauge is accompanied by ringing with a frequency of ~100 000 Hz. This is not due to the through-thickness ring-up time of the gauge, which is ~200 ns. Also, it is not thought to be due to wave reverberations in the clay pipe because the amplitude of the gauge ringing is not reproducible. Rather, it is a consequence of nonplanar shock impact on the gauge which produces structured normal mode vibrations in the lithium niobate disc. The natural frequencies of an elastic disc of radius a and thickness h are given by (10)

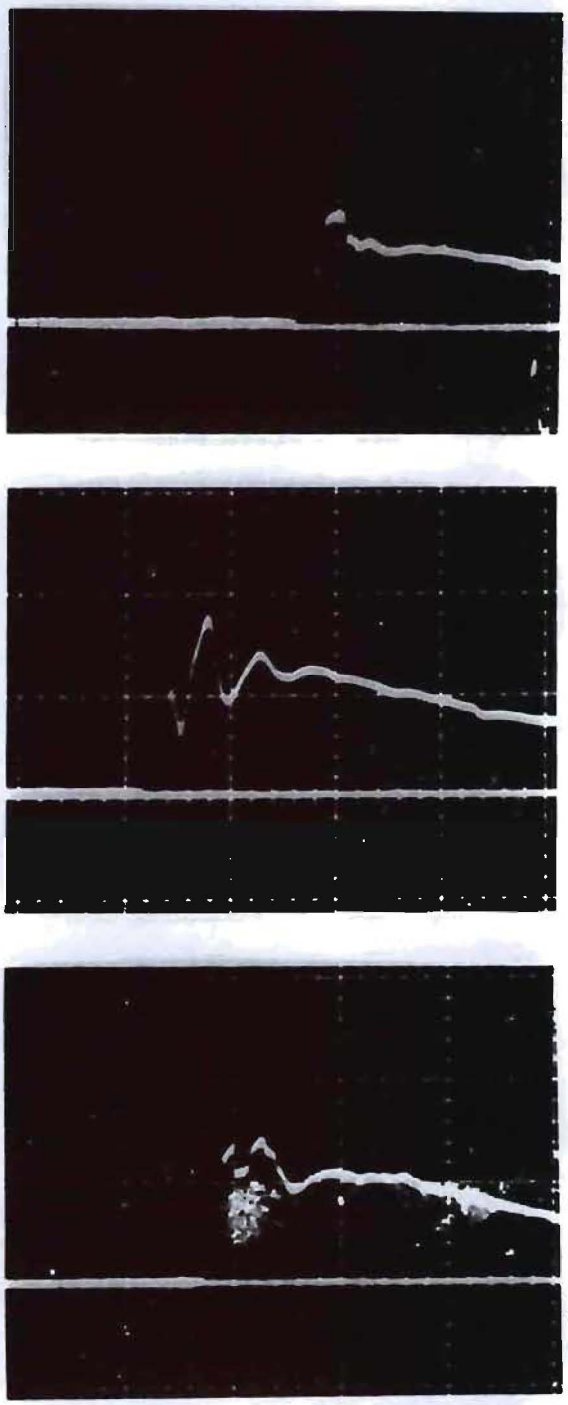

Fig. 4 - Lithium niobate gauge records for aquarium tests C-5084 (top), C-5088 (center), and C-5097 (bottom). The verticle scale is 5 V (2.5 kbar) per division and the horizontal scale is 20 μs per division.

$$\omega_{ns} = \frac{\lambda_{ns}(h/a)}{t_d\sqrt{3(1 - \nu^2)}} \quad , \qquad (2)$$

where ν is Poisson's ratio, t_d is the transit time of a bar wave (one-dimensional stress) across a diameter, and λ_{ns} are tabulated nondimensional constants determined by zeros of Bessel functions.

For 6.35-mm-diameter lithium niobate discs, $t_d \sim 1$ μs, and the natural periods of oscillation are

$$T_{ns} = 2\pi/\omega_{ns} \approx 100/\lambda_{ns} \ (\mu s) \quad , \qquad (3)$$

when the appropriate material and geometrical parameters are substituted into Eq. (2). The first three lowest frequency modes of vibration correspond to periods of ∿20 μs, ∿10 μs, and ∿5 μs. Therefore, we conclude that oscillations in the pressure transducer records are due to normal mode plate vibrations which are ignored in the data reduction.

Figure 5 shows pressure-time records for shots C-5084, C-5088, and C-5097 superimposed on each other with the ringing artificially removed. The time scales have been shifted to give common shock arrival times. It is clear from this figure that not only are peak pressures greater in the cases of 11% and 19% aluminum, but the pressures remain higher in the region behind the shock wave.

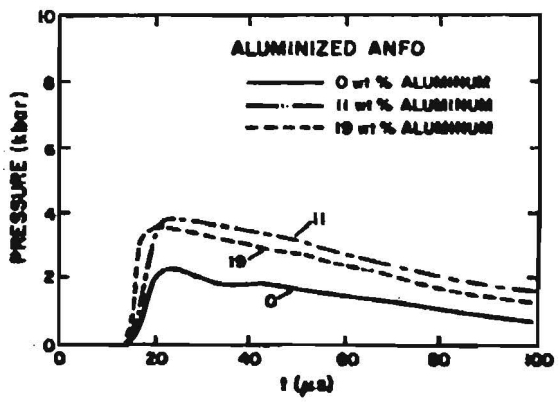

Fig. 5 - Lithium niobate pressure histories (with ringing averaged out) for aquarium tests C-5084 (0% aluminum), C-5088 (11% aluminum), and C-5097 (19% aluminum.

CONCLUSIONS

The aquarium test is shown to be a very useful method for the quantitative study of explosive performance. This is especially true with the addition of the lithium niobate transducer to measure the dynamic pressures in the water.

The aquarium test has been used here to investigate the role of aluminum addition to ANFO. There never has been serious doubt that aluminum increased the total energy of the explosive. The only question was whether or not the initial shock pressure imparted to the surrounding medium was affected by aluminum content. This has clearly been shown to be the case.

As the study of explosive rock breakage continues to reveal the factors controlling the dynamic fracture process, information of the type presented here will be helpful in tayloring commercial explosives for various field situations including borehole size, depth of burial, rock type, and desired fragment size. Economic considerations can also be dealt with more objectively following accurate quantification of explosive performance.

ACKNOWLEDGMENTS

The authors wish to thank R. A. Graham (Sandia National Laboratories) for his help regarding the use of the lithium niobate pressure transducer. The contributions of B. G. Craig, S. C. Schmidt, J. J. Dick, and J. R. Travis (Los Alamos National Laboratory) are also appreciated.

REFERENCES

1. J. N. Johnson, "Calculation of Explosive Rock Breakage: Oil Shale," Proceedings of the 20th Symposium on Rock Mechanics, U.S. National Committee for Rock Mechanics, pp. 109-118, June 1979.

2. T. F. Adams, S. C. Schmidt, and W. J. Carter, "Permeability Enhancement Using Explosive Techniques," ASME Transactions Journal of Energy Resource Technology, forthcoming.

3. S. L. McHugh, D. R. Curran, and L. Seaman, "The NAG-FRAG Computational Fracture Model and its Use for Simulating Fragmentation and Fracture," Proceedings of the Society for Experimental Stress Analysis, 1980 Fall Meeting, pp. 86-97. Oct. 1980.

4. D. E. Grady and M. E. Kipp, "Continuum Modelling of Explosive Fracture in Oil Shale," Int. J. Rock Mech. Min. Sci. and Geomech. Abstr., 17, pp. 147-157, 1980.

5. B. G. Craig, J. N. Johnson, C. L. Mader, and G. F. Lederman, "Characterization of Two Commercial Explosives," Los Alamos Scientific Laboratory report LA-7140, May 1978.

6. R. A. Graham, "Lithium Niobate Stress Transducers," Sandia Technology, Sandia Laboratories, pp. 19-23, Autumn 1975.

7. R. A. Graham and R. P. Reed, eds., "Selected Papers on Piezoelectricity and Impulsive 'Pressure' Measurements," Sandia Laboratories report SAND 78-1911, Dec. 1978.

8. O. G. Winslow, W. C. Davis, and W. C. Chiles, " Multiple-Exposure Image-Intensifier Camera," Proc. 6th Symposium on Detonation, pp. 197-200, August 1976.

9. C. L. Mader, Numerical Modeling of Detonations," University of California Press, Berkeley, 1980, pp. 333-352.

10. W. Flugge, Handbook of Engineering Mechanics, McGraw-Hill Book Co., New York, 1962, pp. 61-62, 61-24.

11. L. D. Landau and E. M. Lifshitz, Fluid Mechanics, Pergamon Press, London, 1959, pp. 317-319.

12. S. P. Marsh, LASL Hugoniot Data, University of California Press, Berkeley, 1980, pp. 573-574.

APPENDIX

The pressure at the shock front in the water can be calculated from the angle the shock front makes with the cylinder axis and the equation of state of water.

As the detonation front moves downward at speed D, the shock front in the water moves normal to itself at speed U. If θ is the angle between the shock front and the cylinder axis, as shown in Fig. 6, and the wave is steady (i.e., propagating without change in shape), then

$$U = D \sin\theta \quad . \tag{4}$$

In Fig. 6 $\hat{n}$ and $\hat{t}$ are unit vectors normal and parallel, respectively, to the shock front at point A. Let u and v be particle velocity components in the $(\hat{n},\hat{t})$ coordinate system, ρ the material density, p the pressure, and e the internal energy per unit mass. Then, if u, v, ρ, p, and e represent flow variables immediately behind the shock, the Rankine-Hugoniot jump conditions (11) give

$$\rho u = -\rho_0 D \sin\theta \quad , \tag{5}$$

$$v = D \cos\theta \quad , \tag{6}$$

$$p + \rho u^2 = \rho_0 D^2 \sin^2\theta \quad , \tag{7}$$

$$(u^2 + v^2)/2 + e + p/\rho = D^2/2 \quad , \tag{8}$$

where ρ_0 is the undisturbed density of the material ahead of the shock (at zero pressure and zero internal energy). From Eqs. (5)-(8), the internal energy change across the oblique shock of Fig. 6 is given by

$$e = (p/2)(1/\rho_0 - 1/\rho) \quad , \tag{9}$$

which is exactly the same as that for a normal shock. Therefore, the pressure-volume states for the oblique shock lie on the Hugoniot curve determined by one-dimensional plane shock-wave experiments. Thus,

$$p = \frac{\rho_0 c_w^2 \epsilon}{(1 - s\epsilon)^2} \quad , \tag{10}$$

where $\epsilon \equiv 1 - \rho_0/\rho$, $\rho_0 = 1.0$ g/cm^3, $c_w = 0.148$ cm/μs is the acoustic (low amplitude sound) wave in water, and $s = 2.0$ is the slope of a straight-line fit to the shock velocity-particle velocity data for water (12). From Eqs. (5) and (7), it is found that

$$p = \rho_0 D^2 \sin^2\theta\epsilon \quad , \tag{11}$$

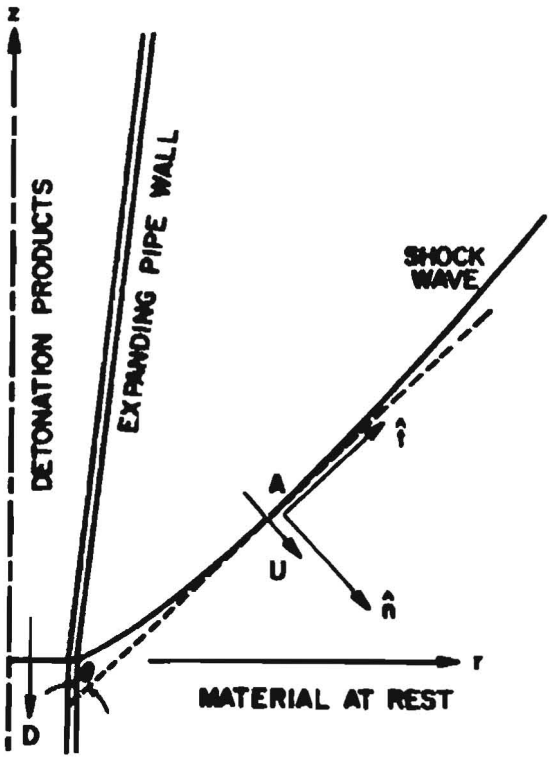

Fig. 6 - Definition of angle θ and coordinate axes for analysis of peak pressure at the pipe wall.

and hence, from Eqs. (10) and (11),

$$p = \rho_0 D^2 \sin^2\theta (1/s)[1 - c_w/(D \sin\theta)] \quad , \tag{12}$$

which gives the pressure behind the shock wave when the steady detonation speed D and the angle θ between the shock and the cylinder axis are known.

The angle θ at the pipe wall is obtained by making a least squares fit to the shock front data in the form $r = f(z)$ and $dr/dz = \tan\theta$ is evaluated at the pipe/water interface. Equation (12) is then used to evaluate the peak shock pressure at the outer wall of the pipe.